

Secular evolution and cylindrical rotation in boxy/peanut bulges: impact of initially rotating classical bulges

Kanak Saha*, & Ortwin Gerhard

Max-Planck-Institut für Extraterrestrische Physik, Giessenbachstrae, D-85748 Garching, Germany

Accepted xxxx Month xx. Received xxxx Month xx

ABSTRACT

Boxy/peanut bulges are believed to originate from galactic discs through secular processes. A little explored question is how this evolution would be modified if the initial disc was assembled around a preexisting classical bulge. Previously we showed that a low-mass initial classical bulge (ICB), as might have been present in Milky Way-like galaxies, can spin up significantly by gaining angular momentum from a bar formed through disc instability. Here we investigate how the disc instability and the kinematics of the final boxy/peanut (BP) bulge depend on the angular momentum of such a low-mass ICB. We show that a strong bar forms and transfers angular momentum to the ICB in all our models. However, rotation in the ICB limits the emission of the bar’s angular momentum, which in turn changes the size and growth of the bar, and of the BP bulge formed from the disc.

The final BP bulge in these models is a superposition of the BP bulge formed via the buckling instability and the spun-up ICB. We find that the long-term kinematics of the composite BP bulges in our simulations is independent of the rotation of the ICB, and is always described by cylindrical rotation. However, as a result of the co-evolution between bulge and bar, deviations from cylindrical rotation are seen during the early phases of secular evolution, and may correspond to similar deviations observed in some bulges. We provide a simple criterion to quantify deviations from pure cylindrical rotation, apply it to all our model bulges, and also illustrate its use for two galaxies: NGC7332 and NGC4570.

Key words: galaxies: bulges – galaxies: structure – galaxies: kinematics and dynamics – galaxies: spiral – galaxies: evolution

1 INTRODUCTION

The formation of realistic disc galaxies and their evolution has remained a challenging problem to the cold dark matter (CDM) paradigm of galaxy formation (White & Rees 1978). Nevertheless, significant development has occurred in this context in recent years. Cosmological hydrodynamical simulations which include feedback and/or smooth accretion of cold gas through cosmic filaments show that an exponential disc could have assembled either around a classical bulge formed through mergers or as a bulgeless disc galaxy, and survived through the hierarchical assembly (Abadi et al. 2003; Governato et al. 2007; Agertz et al. 2011; Brook et al. 2011, 2012).

Soon after their formation, the clumpy discs observed at high-redshift (Genzel et al 2006) are believed to go through rapid dynamical evolution where minor mergers, streams of inflowing gas triggering burst of star formation and tur-

bulence played dominant roles. As these violent processes become less important and frequent (Hopkins et al. 2010; Lotz et al. 2011), secular processes which operate on longer time scales (typically ~ 10 s of dynamical time scales) are thought to play a significant role in the subsequent evolution of the galaxies (Kormendy & Kennicutt 2004). In the secular phase, the most efficient way a disc galaxy evolves is through forming a bar via disc instability which facilitates the redistribution of energy and angular momentum between the disc, dark matter halo and classical bulge (Debattista & Sellwood 2000; Athanassoula 2003; Saha et al. 2012). As the bar grows stronger, it goes through buckling instability and form boxy/peanut bulges (hereafter, BP) as demonstrated in numerous N-body simulation studies (Combes & Sanders 1981; Pfenniger & Norman 1990; Raha et al. 1991; Martinez-Valpuesta & Shlosman 2004; Debattista et al. 2006; Saha et al. 2012). BP bulges are seen in nearly 50% of edge-on disc galaxies (Lütticke et al. 2000) including our Milky Way and the line-of-sight (LOS) stellar and gas kinematics in many such barred edge-on galax-

* E-mail:saha@mpe.mpg.de

ies show cylindrical rotation (Kormendy & Illingworth 1982; Bureau & Freeman 1999; Falcón-Barroso et al. 2006a), as has also been noted in many N -body simulations of barred galaxies (Combes et al. 1990; Sellwood & Wilkinson 1993; Athanassoula & Misiriotis 2002; Saha et al. 2012). Stellar kinematics from the recently completed Bulge Radial Velocity Assay (BRAVA) survey confirms the cylindrical rotation in the Galactic Bulge (Howard et al. 2009; Kunder et al. 2012). Recent observational analyses, however, show deviations from cylindrical rotation in BP bulges, e.g., NGC5746, NGC1381 (Williams et al. 2011). Deviations from cylindrical rotation is also reported in BP bulges of simulated galaxies due to variation in the viewing angles of the bar (Combes et al. 1990; Athanassoula & Misiriotis 2002). However, it is not clear whether the projection effect is the correct interpretation, or whether a physical mechanism is required to explain the deviations from cylindrical rotation observed in BP bulges.

BP bulges are not only formed out of pure axisymmetric discs but they can also form in axisymmetric discs assembled around classical bulges (Saha et al. 2012). Such classical bulges are presumably have formed as a result of violent processes e.g., dissipative collapse (Eggen et al. 1962) or mergers (Baugh et al. 1996). In observation, one does find both barred and unbarred galaxies with classical bulges (Laurikainen et al. 2007). Classical bulges are indeed abundant in disc galaxies and they are known to rotate (Kormendy & Illingworth 1982; Cappellari et al. 2007). In a previous paper, Saha et al. (2012) showed how an initially non-rotating low-mass classical bulge spun-up during the secular evolution and discussed the possible implication it might have on the final BP bulge. Such a low-mass classical bulge ($\sim 8\%$ of disc mass) might be present in the Milky Way as suggested by the N -body modelling of BRAVA stellar kinematics; models with increased bulge masses are shown to produce larger deviation from the data (Shen et al. 2010).

The goal of this paper is to understand the effect of angular momentum of a low-mass ICB on the disc instability and kinematics of the final BP bulge. In particular, does the cylindrical rotation in BP bulges depend on the angular momentum of the ICB and could this possibly explain the deviation from cylindrical rotation in observed BP bulges? Here, we study the formation and growth of a bar and BP bulge in galaxies with a low mass rotating ICB using high resolution N -body simulations. We find that the kinematics of the final BP bulge varies with time but the long-term asymptotic behaviour of the resulting BP bulge does not depend on the initial rotation. We show how cylindrical rotation in BP bulges changes during the secular evolution and devise a method to quantify it.

The paper is organized as follows. Section 2 outlines the initial galaxy model and set up for the N -body simulation. Bar growth and the formation of BP bulges are described in section 3. Kinematics of boxy bulges are described in section 4. Conclusions are presented in section 5.

2 GALAXY MODELS WITH INITIALLY ROTATING CLASSICAL BULGES

Equilibrium models of galaxy with ICBs are constructed using the self-consistent method of Kuijken & Dubinski

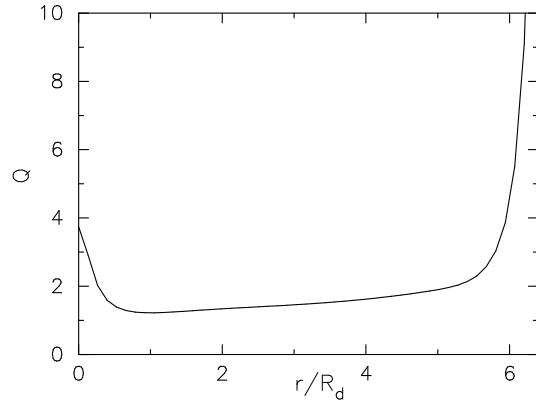


Figure 1. Radial profile of Toomre Q for the initial stellar disc.

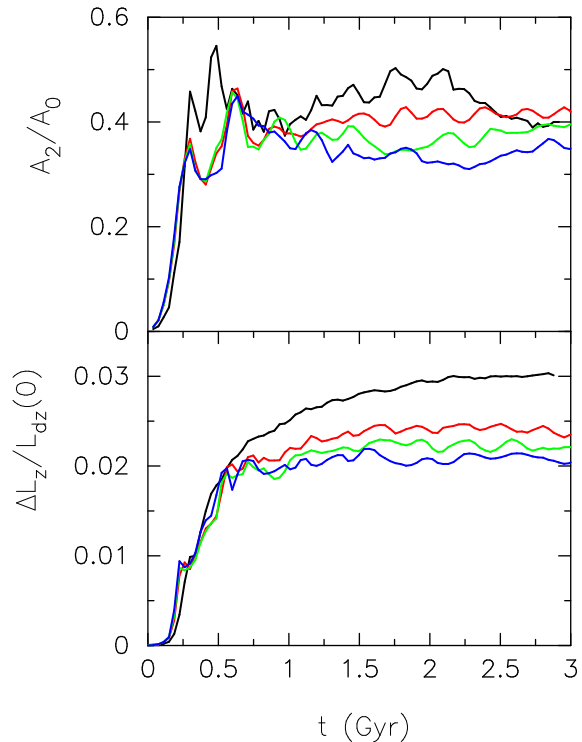


Figure 2. Top panel showing the time evolution of the bar strength in galaxy models with a preexisting spinning classical bulge. Bottom panel shows the net gain of angular momentum by the preexisting classical bulge. $L_{dz}(0)$ denotes the disc specific angular momentum at $T=0$. Black lines in both panels denote the model with non-rotating ICB (RCG004-0). Red (RCG004-A), green (RCG004-B) and blue (RCG004-C) lines in both panels indicate models with rotating ICBs.

(1995). We construct here three galaxy models with rotating ICBs and one with non-rotating ICB RCG004-0 taken from Saha et al. (2012) for comparison. Each of these initial models consists of a live disc, halo and bulge. The initial disc has an exponentially declining surface density with a scale-length R_d , mass M_d and Toomre $Q = 1.4$ at $2.5R_d$ (see Fig. 1 for the radial variation). The live dark matter halo is modelled with a lowered Evans model and the ICB with a King model and general details about the model parameters can be found in (Saha et al. 2010; Saha et al. 2012). The initial parameters for disc, halo and ICB are identical

to model RCG004 of Saha et al. (2012) and the circular velocity curve is the same as presented in Fig. 1 of Saha et al. (2012). The ICBs are strongly flattened by the disc potential (Barnes & White 1984). The ICB in the constructed models has a total mass $M_b = 0.066M_d$ and the initial ellipticity in edge-on projection is $\epsilon_b = 0.465$.

The rotating flattened models of ICBs are constructed by reversing the velocities of particles with negative angular momenta, which remains a valid solution of the collisionless Boltzmann equation (Lynden-Bell 1962). In this way, three models with rotating ICBs which we denote as RCG004-A, RCG004-B and RCG004-C are constructed. Their initial velocity contours are shown in section 4. Model RCG004-A were constructed by randomly changing the corotating fraction (i.e., a fraction of bulge orbits corotating with the disc) to 0.75 (note, corotating fraction = 0.5 generates a non-rotating bulge) and it shows some amount of cylindrical rotation in the central region, although the ICB is axisymmetric (Rowley 1988). Models RCG004-B and RCG004-C were constructed slightly differently based on the work of Dehnen & Gerhard (1993), in that we reversed the velocities of bulge stars belonging to a certain range of angular momenta, especially avoiding the meridional loop orbits, see Fig. 3 of Dehnen & Gerhard (1993).

The initial $(V_m/\bar{\sigma})^*$ values for all the model bulges are shown in Table 1, where V_m is the maximum velocity and $\bar{\sigma}$ is the average velocity dispersion inside the bulge half mass radius. The * sign denotes that values are normalized to the corresponding oblate isotropic rotator model (Binney 1978).

We scale the models such that $M_d = 4.58 \times 10^{10} M_\odot$ and $R_d = 4.0$ kpc. Then the time unit is given by 24.9 Myr. We use a total of 6×10^6 particles to simulate RCG004-A, RCG004-B and RCG004-C whereas for RCG004-0 a total of 10×10^6 particles were used. The softening lengths for the disc, bulge and halo particles used are 12, 5 and 20 pc respectively following the suggestion of McMillan & Dehnen (2007). These simulations are performed using the Gadget code (Springel et al. 2001) with a tolerance parameter $\theta_{tot} = 0.7$, integration time step ~ 0.4 Myr. All the models are evolved for a time period of ~ 3.0 Gyr.

3 SIZE AND GROWTH OF BARS AND BOXY/PEANUT BULGES

Non-linear growth of a bar depends on the amount of angular momentum transferred from the inner region of the stellar disc to the outer disc, to a classical bulge (if exists) and to the surrounding dark matter halo in the host galaxy, all of which act like a sink. In this section, we focus on the effect of a rotating ICB on the size and growth of a bar and the final BP bulge.

All 4 models described in section 2 rapidly form a bar in the disc. In the upper panel of Fig. 2, we show the evolution of the bar amplitude (defined as the maximum of the $m = 2$ Fourier coefficient A_2 normalized to the axisymmetric component A_0) as a function of time for the four models. The net amplitude of the bar is lower in models with classical bulges having higher $(V_m/\bar{\sigma})^*$. Such a decrement in the bar amplitude correlates well with the transfer of angular momenta to the bulge as shown in the bottom panel of Fig. 2. It shows the time evolution of the net gain of specific angular

momentum normalized to the disc's initial angular momentum. The fast rotating ICB absorbs less angular momentum after ~ 1 Gyr as compared to the moderately rotating or non-rotating ICB. The most striking difference is between the fast rotating and non-rotating ICBs; after ~ 1 Gyr, the non-rotating ICB gains ~ 1.5 times more angular momentum than the fast rotating one (see Fig. 2). Note that the linear growth rate of the bar is nearly unaffected by the initial rotation of the classical bulge.

Fig. 3 shows the surface density maps of the inner $2R_d$ regions for all the 4 galaxy models at the end of 2.9 Gyr. In the face-on projection, they show strong bars and in the edge-on projection BP bulges. We measure the bar size using two methods: one using the drop in the ellipticity profile obtained using the IRAF ellipse fitting task on the FITS image (see Fig. 3) generated from the particle model. In the second, we use the radius at which the corresponding position angle of the bar deviates by ~ 5 deg (Erwin 2005). We quote the bar sizes (denoted by R_{bar}) as the minimum of these two measurements obtained at the end of 2.9 Gyrs (see Table 1). For a list of methods on bar size measurement, see Athanassoula & Misiriotis (2002). We have also used an independent method to derive the bar size directly from the particle model. In that, we use the FWHM of the radial profile of the bar amplitude as one measurement and the radius at which the phase angle of the bar deviates by 5 deg as the second. The minimum of these measurements is nearly the same as that obtained from the ellipse fitting method. From these measurements, it is found that the bar sizes are, in general, smaller if the ICB is rotating. On average, for the low mass ICBs considered here rotating with a $(V_m/\bar{\sigma})^* \sim 0.42 - 0.72$, we found about 10 – 40% reduction in the bar size compared to the non-rotating case.

The size of a BP bulge is calculated by finding zeros of the function $D_g(x, z)$ defined as

$$D_g(x, z) = \frac{\Sigma_{los}(x, z) - \Sigma_{los}(0, z)}{\Sigma_{los}(0, z)}, \quad (1)$$

for a set of smoothed surface density (Σ_{los}) profiles (see Fig. 4) along slits parallel to the major axis (x) of a galaxy model such as shown in the lower panels of Fig. 3.

The shape of the function D_g varies along the vertical direction. Close to the midplane (i.e., $z = 0$) of the galaxy, D_g is convex with the zeros occurring at $x = 0$ (i.e., along the minor axis) and values of D_g are always negative at $x \neq 0$. Slightly above the midplane (e.g., $z = 0.11R_d$ in Fig. 4) $D_g = 0$ in the inner regions ($x \sim 0.1R_d$) of some models and smoothly goes to negative beyond that. We define such a profile as characteristic of a boxy shaped bulge. At higher values of z (e.g., at $z = 0.23, 0.3R_d$, in Fig. 4) the shape of the function D_g takes the form of a characteristic peanut shape. Above $z = 0.3R_d$, we find that shape of the function D_g becomes irregular for some models and makes it harder to compare them with other models. We consider the profiles at $z = 0.3R_d$ to compute the length of the BP bulge for all the models. The length of the BP bulge (denoted by BPL , see Lütticke et al. (2000)) is obtained by calculating the distance between two zeros of the function D_g on either side of the galaxy centre and they are enlisted in Table 1. This method reliably returns the values of BPL as a function of vertical height (z) when there is a clear peanut signature

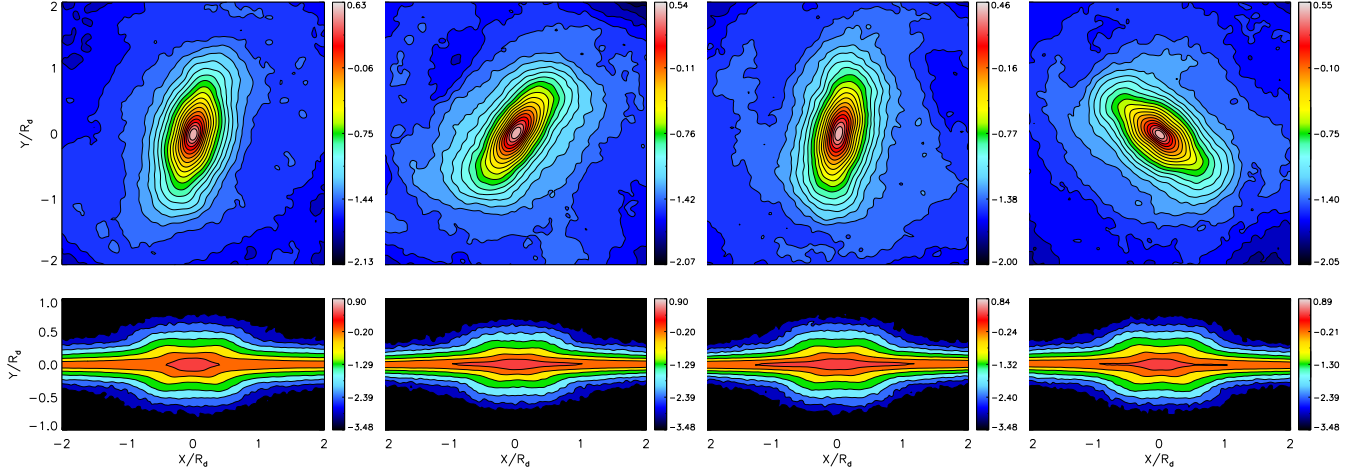


Figure 3. Bars and boxy/peanut bulges at the end of 2.9 Gyrs. From left to right, the models are RCG004-0, RCG004-A, RCG004-B and RCG004-C. Initial rotation of the classical bulge increases from left to right. Bottom panels show side-on projections of the models, above, along the short axis in the galactic plane.

and it is found that the largest BP bulge forms in model RCG004-0 with non-rotating ICB.

The strength of the BP bulge in our models is obtained by calculating the maximum of the $m = 2$ Fourier coefficient (denoted by $C_{2,z}^{max}$) of the z -coordinates of the disc particles belonging to the bar (Martínez-Valpuesta & Athanassoula 2008). In order to understand the effect of ICB on the disc, we have used only disc particles to compute A_2 and $C_{2,z}$. The values of $C_{2,z}^{max}$ are shown in Table 1. It is found that the strength of BP bulges in our models with non-rotating ICB and fast rotating ICB are nearly the same. However, with moderately or slowly rotating ICBs, the strength is lowered by $\sim 20 - 40\%$.

Further, we perform a 2D bulge-disc decomposition on the FITS images produced from our simulations using GALFIT (Peng et al. 2002) and derive the bulge half mass radii ($R_{b,1/2}$), sersic indices (n_b) (see Table 1) and ellipticities for all the four final BP bulges shown in Fig. 3. Note that the BP bulge here is a composite bulge which is a superposition of the BP bulge formed out of the disk material and the ICB at 2.9 Gyrs. The initial value of $R_{b,1/2}$ for the non-rotating ICB is $0.26R_d$. We do not find any definite trend either in the sersic indices or bulge sizes with the initial rotation in the classical bulges but the slowly rotating one in our model (RCG004-A) forms shorter bulge and have larger sersic index.

4 KINEMATICS OF BOXY/PEANUT BULGES

Kinematically BP bulges are distinguished from the classical bulges in that BP bulges possess cylindrical rotation as observed in a number of external galaxies (Kormendy & Illingworth 1982; Falcón-Barroso et al. 2006b) as well as in our Milky Way (Howard et al. 2009) but see Williams et al. (2011) for exceptional cases which displayed noticeable deviation from cylindrical rotation. All four models of BP bulges, studied here, rotate cylindrically

Table 1. Rotating ICBs and properties of bars and boxy/peanut bulges at 2.9 Gyr in our simulations. Symbols are explained in section 2 and 3.

Galaxy models	$(V_m/\sigma)^*$ (at $T=0$)	R_{bar} ($\times R_d$)	$R_{b,1/2}$ ($\times R_d$)	n_b	BPL ($\times R_d$)	$C_{2,z}^{max}$
RCG004-0	0.0	1.35	0.32	1.12	1.02	0.085
RCG004-A	0.42	0.95	0.25	1.33	0.74	0.056
RCG004-B	0.52	1.20	0.27	1.13	0.83	0.068
RCG004-C	0.72	1.10	0.33	1.03	0.86	0.084

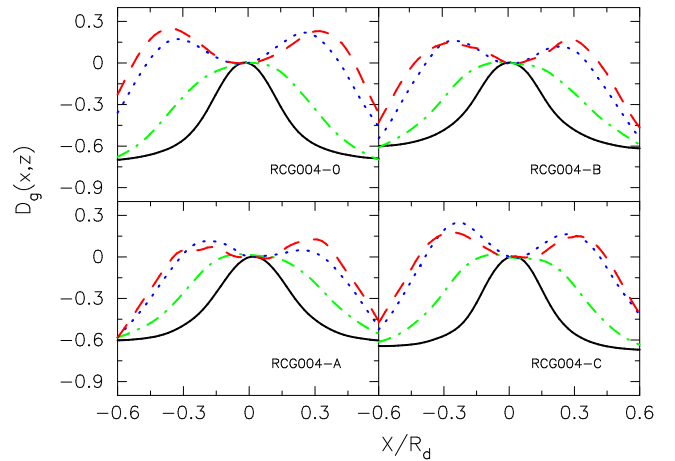


Figure 4. Shape of the function D_g along slits parallel to the major axis for all the four models. In each panel, profiles are drawn at $z/R_d = 0.009$ (solid black line), 0.11 (green dashed-dot line), 0.23 (blue dotted line), and 0.3 (red dashed line). The profiles at $z/R_d = 0.3$ are used here to measure the size of the boxy/peanut bulges.

but the degree of cylindrical rotation is seen to be varying with time as the model galaxy evolves. In section 4.1, we provide a simple prescription to quantify the degree of cylindrical rotation. The current section is focused on understanding how the kinematics of the BP bulges depend on the initial rotation in the ICBs.

In Fig. 5, we show mean LOS velocity profiles along slits placed parallel to the major axis of our galaxy model to probe how the rotation of a BP bulge varies along the vertical direction. At the end of 2.9 Gyrs, all the models exhibit clear (see section 4.1 for numbers) cylindrical rotation up to a height of $\sim 0.23R_d$ ($\simeq R_{b,1/2}$) which is about 900 pc for the adopted scaling above the galactic midplane. Unlike models with rotating ICBs, the model with non-rotating ICB (RCG004-0) show cylindrical rotation up to a height of ~ 1200 pc above the midplane. This is also clear from the 2D velocity contours of the BP bulge region as depicted in Fig. 6. In models with rotating ICBs, the velocity contours start deviating above a height of $\sim 0.25R_d$. Fig. 6 reveals that, although the initial bulge rotation for all the four models are quite different, at the end of 2.9 Gyrs they show similar kinematics. It remains to verify whether their evolutionary paths are also nearly identical. We address this issue in section 4.1.

In Fig. 7, we show the variation of mean velocity dispersion (σ_{los}) of stars in the final BP bulge along the vertical direction at two different radii from the centre of the respective galaxy model. In all the models, the minor axis σ_{los} profiles show steeper vertical gradient than the profiles at $X = 0.17R_d$ (which is well within the bulge half-mass radii). A vertical gradient in the stellar velocity dispersion is observed in classical bulges as well as in boxy bulges (Williams et al. 2011). It has also been observed that the velocity dispersion is remarkably constant along vertical direction in NGC4594 (a classical bulge) and in the well known boxy bulge of NGC4565 (Kormendy & Illingworth 1982). So a gradient in the velocity dispersion does not necessarily indicate the nature of the underlying bulge. If measured in the boxy bulge region, one would perhaps expect a shallow gradient in the velocity dispersion. From Fig. 7, it is clear that the rotation of the low mass ICBs does make little difference in the velocity dispersion of the final BP bulge.

4.1 Criteria for cylindrical rotation

By definition, cylindrical rotation means that the mean LOS velocity $V_{los}(x, z)$ of stars at a particular distance (x) from the centre is independent of its vertical height (z) i.e., zero vertical gradient ($dV_{los}(x, z)/dz = 0$). This is approximately true for observed barred galaxies as well as for bulges in N-body simulations (Combes et al. 1990; Athanassoula & Misiriotis 2002). Here, we construct a simple criterion for measuring the degree of cylindrical rotation in BP bulges.

We consider again a set of slits, nearly covering the vertical extent of the BP bulge, parallel to the major axis in edge-on projection. Along these slits, we have the LOS surface density $\Sigma_{los}(x, z)$ and velocity $V_{los}(x, z)$ of stars. For a given slit placed at $z = z_i$, we can compute the mass weighted line-of-sight velocity for all the stars within a projected distance X_j from the minor axis of the edge-on image. This quantity may be normalized by replacing the in-

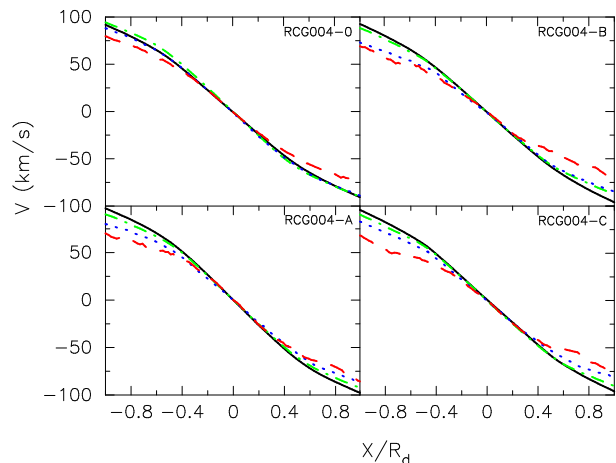


Figure 5. The mean LOS velocity profiles along 4 different slits placed at $z/R_d = 0.009$ (solid black line), 0.11 (green dashed-dot line), 0.23 (blue dotted line), and 0.35 (red dashed line) are shown in each panel. All the velocity profiles are shown for $T = 2.9$ Gyr. Cylindrical rotation is evident within the bulge half-mass radii of all models and extends beyond $R_{b,1/2}$ for the model with non-rotating ICB (RCG004-0).

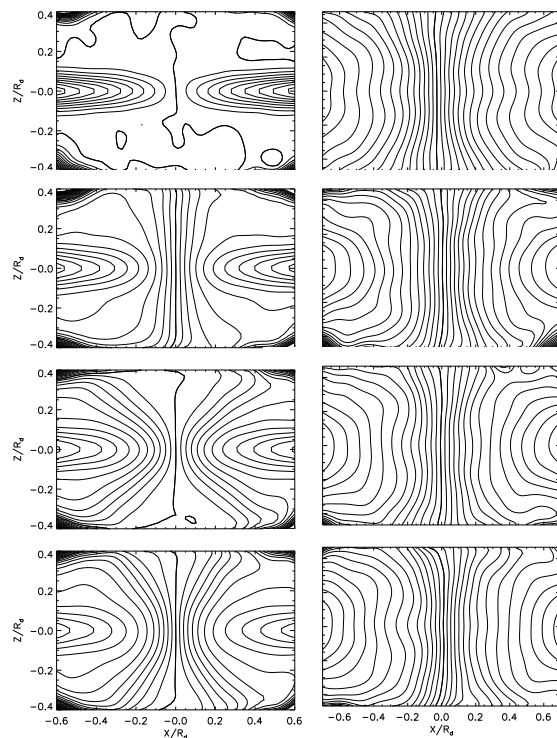


Figure 6. Spider diagrams for the mean LOS velocity of stars in the boxy bulge region which includes stars from the disk as well. From top to bottom, panels are drawn for models RCG004-0, RCG004-A, RCG004-B and RCG004-C. From left to right panels, they show evolution of the velocity structure between initial ($T=0$) and final states ($T=2.9$ Gyr).

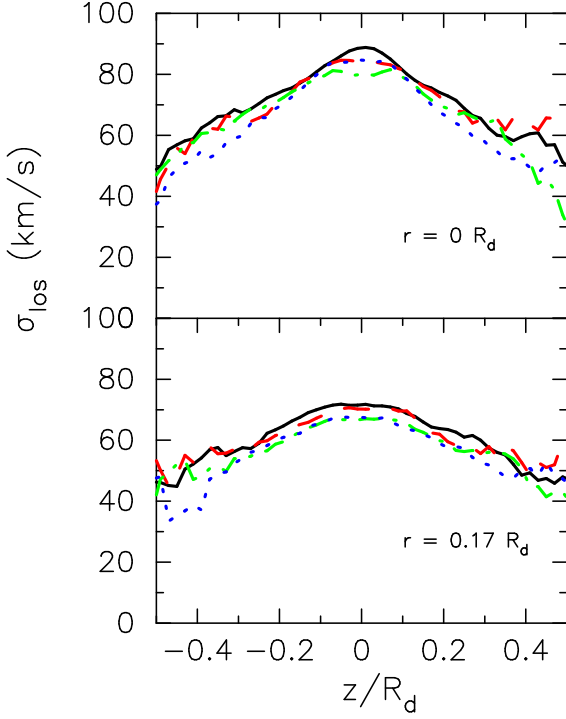


Figure 7. The vertical profiles of LOS velocity dispersion at different locations from the centre of the galaxy. The upper panel shows the dispersion profiles along the minor axis while the bottom panel shows for $X = 0.17R_d$. In both panels, solid black lines denote RCG004-0, green dash-dot lines denote RCG004-A, blue dotted lines RCG004-B and red dashed lines RCG004-C. All the dispersion profiles are derived at $T = 2.9$ Gyr.

dividual velocities of all the stars within X_j with a velocity at the bulge half-mass radius close to the disc midplane $V_{los}(R_{b,1/2}, z \simeq 0)$. After some experimenting, we adopt a weighting scheme and define a dimensionless quantity for the given slit as follows:

$$\delta_{CL}(z, X_j) = \frac{\int_0^{X_j} \Sigma_{los}(x, z) V_{los}(x, z_i) x^2 dx}{V_{los}(R_{b,1/2}, z \simeq 0) \int_0^{X_j} \Sigma_{los}(x, z) x^2 dx}. \quad (2)$$

We compute this quantity for the set of slits considered. The adopted weighting scheme puts more weight on the data points further from the minor axis. Note that, both the numerator and denominator have the dimension of angular momentum. If the stars close to the disc midplane rotate faster than the stars above, the denominator will always be greater than the numerator. If we had the knowledge of de-projection, one could interpret the above formulae as how the average rotational motion of stars associated with an infinitesimally thin disc at a vertical distance $z = z_i$ compares to the one close to the midplane. In general, the values of δ_{CL} are ~ 1 near the midplane and decrease as z increases.

To proceed further, we plot the computed δ_{CL} values against the slit location (z) above the galactic midplane. The velocities of stars decrease along the vertical direction in our model galaxies and the same is expected for galaxies in equilibrium. So we expect δ_{CL} values can be well approximated by a linear function of z , where z is scaled to $R_{b,1/2}$. We then fit a straight line to the (δ_{CL}, z) curve and derive

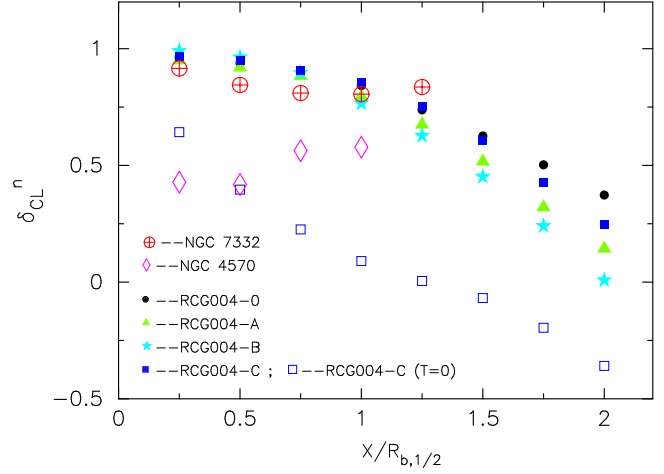


Figure 8. Degree of cylindrical rotation at different major axis radii of our N-body models of BP bulges plotted the end of 2.9 Gyrs. Overplotted here are the degree of cylindrical rotation for two galaxies NGC7332 and NGC4570.

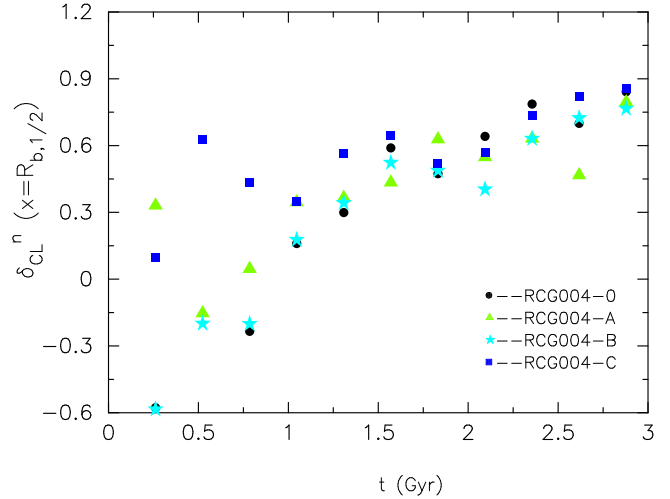


Figure 9. Time evolution of the degree of cylindrical rotation calculated at the bulge half mass radii for four N-body models.

the slope m_{CL} . The degree of cylindrical rotation in the BP bulge is then defined as

$$\delta_{CL}^n(X_j) = 1 + m_{CL}. \quad (3)$$

The values of δ_{CL}^n are generally less than 1 unless δ_{CL} increases in the vertical direction which is unlikely for realistic models of galaxies. Note δ_{CL}^n is undefined for a non-rotating bulge because Eq. 2 would give $\frac{0}{0}$. $\delta_{CL}^n = 1$ denotes pure cylindrical rotation. The degree of cylindrical rotation decreases as the value of δ_{CL}^n decreases from unity. One could carry out the above exercise for different values of X_j (e.g., $X_j = 0.5R_{b,1/2}, R_{b,1/2}, 2R_{b,1/2}$ etc.) and show how the degree of cylindrical rotation in a BP bulge would depend on the chosen value of X_j .

In Fig. 8, we show how the degree of cylindrical rotation varies within the BP bulge at the end of $T = 2.9$ Gyrs. Within $R_{b,1/2}$, all the model BP bulges show nearly the same degree of cylindrical rotation. Beyond the bulge effective radii, δ_{CL}^n decreases rapidly. For the models with mod-

erately rotating bulges (e.g., RCG004-A and RCG004-B), δ_{CL}^n values are systematically lower (see Fig. 8). We have also plotted the values of δ_{CL}^n for the model RCG004-C at $T = 0$ when the bulge showed no sign of cylindrical rotation (see Fig 6).

In order to test the above formulae, we applied it to two real galaxies, NGC7332 and NGC4570. NGC7332 is a well studied galaxy in the literature and shows prominent cylindrical rotation (Falc3n-Barroso et al. 2004). We have used SAURON integral-field kinematics data (Emsellem et al. 2004) for the above two galaxies. The bulge effective radii ($R_{b,1/2}$) for NGC4570 and NGC7332 were taken to be 14 and 6 arcsec respectively (Emsellem et al. 2004; Fisher et al. 1994). Our analysis indicates that NGC7332 has a high degree of cylindrical rotation ($\delta_{CL}^n \geq 0.8$) within the bulge effective radius. On the other hand, NGC4570 shows non-cylindrical rotation within its bulge effective radius (see Fig. 8).

Based on the above measurements of the degree of cylindrical rotation in about 6 bulges, we introduce $\delta_{crit} = 0.75$ as the boundary between cylindrical and non-cylindrically rotating bulges. Note that such a demarcation is not based on any rigorous calculation but should be treated as an operational definition. $\delta_{crit} = 0.75$ separates well, the rotating classical bulge (RCG004-C ($T=0$)) and non-cylindrically rotating spheroidal bulge of NGC 4570 from the rest of our sample. So a model bulge with $\delta_{CL}^n > \delta_{crit}$ ($\delta_{CL}^n < \delta_{crit}$) would be described as a *cylindrical rotator* (otherwise). It would be interesting to investigate $\delta_{CL}^n(X = R_{b,1/2})$ for a larger sample of boxy bulges.

4.2 Time dependent cylindrical rotation

In Fig. 6, we showed that the kinematics of BP bulges at the end of 2.9 Gyrs turned out to be similar and independent of the initial rotation of the ICBs. Here, we compute the degree of cylindrical rotation within the bulge effective radius as a function of time for all the four models and plotted them in Fig. 9. This figure reveals interesting evolutionary behaviour for the BP bulges. First of all, Fig. 9 shows clearly that the degree of cylindrical rotation varies with time and that there are substantial differences at early times depending on the initial rotation of the ICBs. Nevertheless, irrespective of the initial condition, each model BP bulge evolves towards attaining a higher degree of cylindrical rotation and within their respective bulge effective radii, the values of δ_{CL}^n approach the same level. From Fig. 9, we notice that it takes about 2.0 Gyr since the buckling episode for the cylindrical rotation to be present at the level of $\delta_{CL} \geq 0.75$ in our model bulges. In the section below, we show a snapshot during the evolution at $T = 1.05$ Gyr when cylindrical rotation in the bulge is still developing.

4.3 Boxy/peanut bulges with non-cylindrical rotation

Non-cylindrically rotating boxy bulges are seen in some galaxies e.g., NGC1381, NGC5746 and IC4767 (Williams et al. 2011). It is not clear what might have caused such boxy bulges to rotate non-cylindrically.

The analysis of the previous section demonstrate that

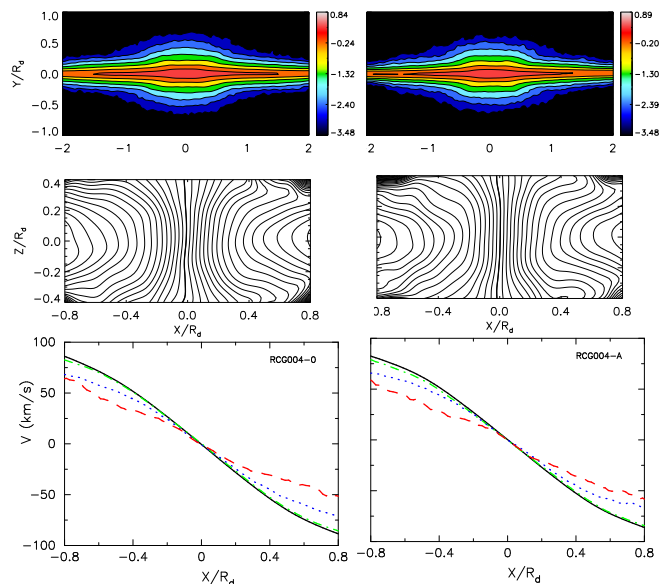


Figure 10. Top panels showing the surface densities for two models RCG004-0 (left) and RCG004-A (right) at $T=1.05$ Gyr. The middle panels show the contours of the 2D mean LOS velocity field for both the models. Velocity profiles at 4 different slits placed at $z/R_d = 0.0$ (black solid line), 0.11 (green dash-dot line), 0.23 (blue dotted line) and 0.35 (red dashed line) parallel to the major axis of the galaxy are depicted in the bottom panels. Both models show deviations from pure cylindrical rotation within their respective bulge half-mass radii.

the kinematics of BP bulges are time-dependent, especially the degree of cylindrical rotation. From Fig. 9, we see that at $T = 1.05$ Gyr beyond the buckling instability phase, two of the model bulges have less cylindrical rotation than the other two. In Fig. 10 and Fig. 11, we show the surface density and kinematics of all four model galaxies at $T = 1.05$ Gyr. According to our convention for δ_{crit} , all 4 models of BP bulges at this time are non-cylindrically rotating. Note however, that the BP bulge in RCG004-C (see Fig. 11) has cylindrical rotation within a smaller region about the minor axis. Since $\delta_{CL}^n(X = R_{b,1/2})$ refers to the bulk of the bulge, such small details are averaged out. The present analysis indicates that boxy bulges with non-cylindrical rotation could still be in their early phase of evolution i.e., have formed relatively recently in their host galaxies. Another possibility is that in those galaxies the ICB was too massive to be spun-up all the way to cylindrical rotation; the response of massive ICBs to a growing bar will be investigated in a future publication.

As shown in section 3, all the rotating and non-rotating ICBs gain angular momentum emitted by the bar. As a result of the angular momentum gain, the ICBs spin up and their orbital structures evolve over time. A spherical harmonics analysis of the 3D density distribution of the ICBs showed that their inner regions formed a bar-like structure. For details on the case of non-rotating ICB (here, model RCG004-0), the readers are referred to Saha et al. (2012). The inner regions of these ICBs exhibit cylindrical rotation beyond about 0.5 Gyr which marks the bar buckling instability phase in the disc. The net cylindrical rotation in the composite bulges (e.g., shown in Fig. 3, Fig. 10 or Fig. 11)

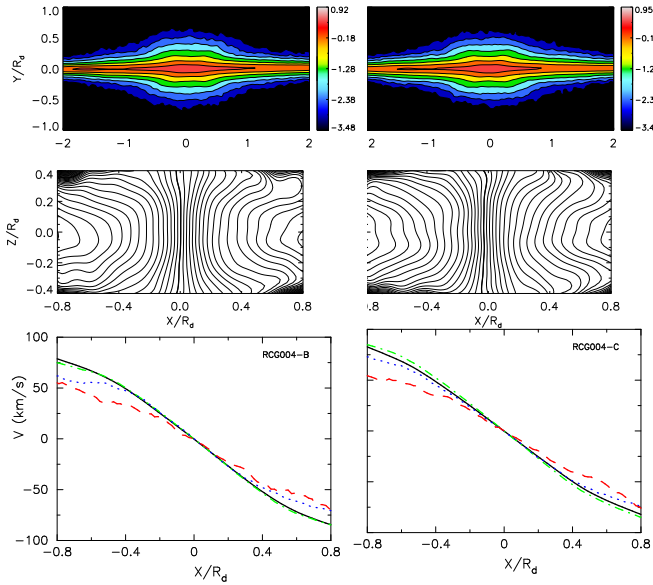


Figure 11. Same as in Fig. 10 but for models RCG004-B (left) and RCG004-C (right).

has its contribution from the evolved rotating ICB and the boxy bulge that form out of the bar buckling instability.

5 CONCLUSIONS

We have investigated the morphology and kinematics of a BP bulge that results from the instability of an axisymmetric disc assembled around a rotating low-mass ICB during the galaxy formation process. The composite BP bulge in our model contains a rotating ICB and shows highly evolving kinematics. Our main conclusions are highlighted below:

1. The size and strength of the bars and resulting BP bulges in our simulations are reduced by $\sim 10 - 40\%$ in galaxy models containing ICBs rotating with $(V_m/\sigma)^* = 0.4 - 0.7$ compared to one with $(V_m/\sigma)^* = 0.0$.
2. Rotating ICBs gain less angular momentum compared to the non-rotating ICB during the secular evolution.
3. We show that cylindrical rotation in BP bulges in our simulations are time-dependent. During the early phases of BP bulge formation, significant deviations from cylindrical rotation can be observed. We quantify such deviations by providing a simple formulae. Our formulae when applied to NGC7332, gives a value for $\delta_{CL}^n = 0.8$ within the bulge half-mass radius. Using the same formulae, we confirm that NGC4570 is not cylindrically rotating.
4. The degree of cylindrical rotation in the composite BP bulges does not depend on the angular momentum of the ICBs sufficiently long time after its formation.
5. The early kinematics of BP bulges with rotating low-mass ICBs in our simulations suggest that the BP bulges with deviation from cylindrical rotation might have formed relatively recently.

ACKNOWLEDGEMENT

KS acknowledges support from the Alexander von Humboldt Foundation and visiting support from IUCAA, Pune. The authors thank the referee Dr. Juntao Shen for constructive comments on the manuscript. The authors would like to thank Michael J. Williams, Chaitra Narayan for useful comments and discussion.

REFERENCES

- Abadi M. G., Navarro J. F., Steinmetz M., Eke V. R., 2003, *ApJ*, 591, 499
- Agertz O., Teyssier R., Moore B., 2011, *MNRAS*, 410, 1391
- Athanassoula E., 2003, *MNRAS*, 341, 1179
- Athanassoula E., Misiriotis A., 2002, *MNRAS*, 330, 35
- Barnes J., White S. D. M., 1984, *MNRAS*, 211, 753
- Baugh C. M., Cole S., Frenk C. S., 1996, *MNRAS*, 283, 1361
- Binney J., 1978, *MNRAS*, 183, 501
- Brook C. B., Governato F., Roškar R., Stinson G., Brooks A. M., Wadsley J., Quinn T., Gibson B. K., Snaith O., Pilkington K., House E., Pontzen A., 2011, *MNRAS*, 415, 1051
- Brook C. B., Stinson G., Gibson B. K., Roškar R., Wadsley J., Quinn T., 2012, *MNRAS*, 419, 771
- Bureau M., Freeman K. C., 1999, *AJ*, 118, 126
- Cappellari M., Emsellem E., Bacon R., Bureau M., Davies R. L., de Zeeuw P. T., Falcón-Barroso J., Krajnović D., Kuntschner H., McDermid R. M., Peletier R. F., Sarzi M., van den Bosch R. C. E., van de Ven G., 2007, *MNRAS*, 379, 418
- Combes F., Debbasch F., Friedli D., Pfenniger D., 1990, *A&A*, 233, 82
- Combes F., Sanders R. H., 1981, *A&A*, 96, 164
- Debattista V. P., Mayer L., Carollo C. M., Moore B., Wadsley J., Quinn T., 2006, *ApJ*, 645, 209
- Debattista V. P., Sellwood J. A., 2000, *ApJ*, 543, 704
- Dehnen W., Gerhard O. E., 1993, *MNRAS*, 261, 311
- Eggen O. J., Lynden-Bell D., Sandage A. R., 1962, *ApJ*, 136, 748
- Emsellem E., Cappellari M., Peletier R. F., McDermid R. M., Bacon R., Bureau M., Copin Y., Davies R. L., Krajnović D., Kuntschner H., Miller B. W., de Zeeuw P. T., 2004, *MNRAS*, 352, 721
- Erwin P., 2005, *MNRAS*, 364, 283
- Falcón-Barroso J., Bacon R., Bureau M., Cappellari M., Davies R. L., de Zeeuw P. T., Emsellem E., Fathi K., Krajnović D., Kuntschner H., McDermid R. M., Peletier R. F., Sarzi M., 2006a, *MNRAS*, 369, 529
- Falcón-Barroso J., Bacon R., Bureau M., Cappellari M., Davies R. L., de Zeeuw P. T., Emsellem E., Fathi K., Krajnović D., Kuntschner H., McDermid R. M., Peletier R. F., Sarzi M., 2006b, *MNRAS*, 369, 529
- Falcón-Barroso J., Peletier R. F., Emsellem E., Kuntschner H., Fathi K., Bureau M., Bacon R., Cappellari M., Copin Y., Davies R. L., de Zeeuw T., 2004, *MNRAS*, 350, 35
- Fisher D., Illingworth G., Franx M., 1994, *AJ*, 107, 160
- Genzel et al 2006, *Nature*, 442, 786
- Governato F., Willman B., Mayer L., Brooks A., Stinson G., Valenzuela O., Wadsley J., Quinn T., 2007, *MNRAS*, 374, 1479

- Hopkins P. F., Croton D., Bundy K., Khochfar S., van den Bosch F., Somerville R. S., Wetzel A., Keres D., Hernquist L., Stewart K., Younger J. D., Genel S., Ma C.-P., 2010, *ApJ*, 724, 915
- Howard C. D., Rich R. M., Clarkson W., Mallery R., Kormendy J., De Propris R., Robin A. C., Fux R., Reitzel D. B., Zhao H. S., Kuijken K., Koch A., 2009, *ApJ*, 702, L153
- Kormendy J., Illingworth G., 1982, *ApJ*, 256, 460
- Kormendy J., Kennicutt Jr. R. C., 2004, *ARA&A*, 42, 603
- Kuijken K., Dubinski J., 1995, *MNRAS*, 277, 1341
- Kunder A., Koch A., Rich R. M., de Propris R., Howard C. D., Stubbs S. A., Johnson C. I., Shen J., Wang Y., Robin A. C., Kormendy J., Soto M., Frinchaboy P., Reitzel D. B., Zhao H., Origlia L., 2012, *AJ*, 143, 57
- Laurikainen E., Salo H., Buta R., Knapen J. H., 2007, *MNRAS*, 381, 401
- Lotz J. M., Jonsson P., Cox T. J., Croton D., Primack J. R., Somerville R. S., Stewart K., 2011, *ApJ*, 742, 103
- Lütticke R., Dettmar R.-J., Pohlen M., 2000, *A&A*, 362, 435
- Lynden-Bell D., 1962, *MNRAS*, 123, 447
- Martínez-Valpuesta I., Athanassoula E., 2008, in J. H. Knapen, T. J. Mahoney, & A. Vazdekis ed., *Pathways Through an Eclectic Universe Vol. 390 of Astronomical Society of the Pacific Conference Series, Boxy/Peanut Bulges and Stellar Bars*. p. 463
- Martínez-Valpuesta I., Shlosman I., 2004, *ApJ*, 613, L29
- McMillan P. J., Dehnen W., 2007, *MNRAS*, 378, 541
- Peng C. Y., Ho L. C., Impey C. D., Rix H.-W., 2002, *AJ*, 124, 266
- Pfenniger D., Norman C., 1990, *ApJ*, 363, 391
- Raha N., Sellwood J. A., James R. A., Kahn F. D., 1991, *Nature*, 352, 411
- Rowley G., 1988, *ApJ*, 331, 124
- Saha K., Martínez-Valpuesta I., Gerhard O., 2012, *MNRAS*, 421, 333
- Saha, K., Tseng, Y., & Taam, R. E. 2010, *ApJ*, 721, 1878
- Sellwood J. A., Wilkinson A., 1993, *Reports on Progress in Physics*, 56, 173
- Shen J., Rich R. M., Kormendy J., Howard C. D., De Propris R., Kunder A., 2010, *ApJ*, 720, L72
- Springel V., Yoshida N., White S. D. M., 2001, *NewA*, 6, 79
- White S. D. M., Rees M. J., 1978, *MNRAS*, 183, 341
- Williams M. J., Zamojski M. A., Bureau M., Kuntschner H., Merrifield M. R., de Zeeuw P. T., Kuijken K., 2011, *MNRAS*, 414, 2163